Scripta Materialia 194 (2021) 113718

Contents lists available at ScienceDirect

Scripta Materialia

journal homepage: www.elsevier.com/locate/scriptamat

Hydrogen uptake and its influence in selective laser melted austenitic stainless steel: A nanoindentation study

Jeong-Min Park[a,1], Yakai Zhao[b,1], Thomas Voisin[c], Dong-Hyun Lee[d], Shin-ichi Komazaki[e], Yoonseok Ko[f,g], Dong-Ik Kim[f], Jin-Yoo Suh[f], Heung Nam Han[g], Y. Morris Wang[c,h,*], Upadrasta Ramamurty[b,*], Jae-il Jang[a,*]

[a] Division of Materials Science and Engineering, Hanyang University, Seoul 04763, Republic of Korea
[b] School of Mechanical and Aerospace Engineering, Nanyang Technological University, Singapore 639798
[c] Materials Science Division, Lawrence Livermore National Laboratory, Livermore, CA 94550, USA
[d] Max-Planck-Institut für Eisenforschung GmbH, Max-Planck-Straße 1, Düsseldorf 40237, Germany
[e] Department of Mechanical Engineering, Kagoshima University, Kagoshima 890-0065, Japan
[f] Center for Energy Materials Research, Korea Institute of Science and Technology, Seoul 02792, Republic of Korea
[g] Department of Materials Science and Engineering, Seoul National University, Seoul 08826, Republic of Korea
[h] Department of Materials Science and Engineering, University of California, Los Angeles, CA 90095, USA

ARTICLE INFO

Article history:
Received 9 December 2020
Accepted 31 December 2020
Available online 8 January 2021

Keywords:
Additive manufacturing
Hydrogen
Nanoindentation
Austenitic stainless steel
Selective laser melting

ABSTRACT

The effect of hydrogen (H) charging on the nanoindentation response of a selective laser melted (SLM) 316L austenitic stainless steel was investigated and compared with its conventionally manufactured (CM) counterpart. Results show that the hardness increment in the SLM samples due to H charging is relatively smaller. Thermal desorption spectroscopy analysis suggests that the charged SLM alloy has not only a smaller H content but a lower apparent H diffusivity in comparison to the CM alloy. This was attributed to the ultrafine solidification cell structure in the SLM alloy. Through the low-load nanoindentation experiments and forward-scattered electron imaging analysis, statistical distributions of the hardness of the cell walls and interiors were assessed. The cell walls, consisting of high-density dislocations with segregated elements, were relatively insensitive to H charging than the cell interiors. These results are discussed in terms of the apparent H solubility and diffusivity in the SLM alloy.

The microstructures of alloys additively manufactured (AM) using either selective laser melting (SLM) or other powder bed fusion (PBF) technologies are distinct in several different ways [1–5]. One of the important microstructural consequences caused by the non-equilibrium processing conditions that prevail during SLM is the presence of an ultrafine solidification cell structure, especially in steels [6,7], superalloys [8], and high-entropy alloys [9,10]. The cell walls mainly consist of high-density dislocations; segregation of alloying elements to the cell walls and fine precipitates in them are also reported. These cells, together with the mesostructures, not only impart a hierarchical nature to the microstructure, but also impart high ductility and toughness without compromising on the strength [6,7,11,12]. In view of such unique features, both in terms of the microstructures and the mechanical performance, detailed understanding of the structure-property correlations in SLM alloys is an active area of current research [1,6,13,14]. While considerable volume of literature is already available on the "general" mechanical properties of SLM alloys at ambient conditions, experimental work on how these alloys behave under "special" service conditions such as in hydrogen (H) environments has not been examined in detail yet [15–19]. The presence of H is known to adversely affect the mechanical performance of most alloys [20–22].

In the conventionally manufactured (CM) 316L stainless steel, a relatively high local H concentration (e.g. near crack tip) is essential for triggering H embrittlement, which depends on both the intrinsic (such as H solubility, diffusivity and trapping states) and extrinsic (such as deformation strain rate and temperature) factors [23–25]. In this regard, it is possible that the cellular structure containing high density of dislocations in SLM alloys can enhance its H absorption capacity and thus exacerbate the H-induced mechanical degradation. We investigate this particular "intrinsic" aspect in this paper through nanoindentation technique that enables local mechanical property evaluation of small-scale features [26–29] like

* Corresponding authors.
E-mail addresses: ymwang@ucla.edu (Y.M. Wang), uram@ntu.edu.sg (U. Ramamurty), jijang@hanyang.ac.kr (J.-i. Jang).
[1] These authors contributed equally to this work.

https://doi.org/10.1016/j.scriptamat.2020.113718
1359-6462/

the cellular structure in SLM alloys. The effects of H charging on the mechanical properties of the SLM 316L stainless steel (SS)—one of the most widely used steel as well as an extensively investigated SLM alloy [6,7,11,30]—are examined and compared with those of its CM counterpart. The results show, surprisingly, that the solidification cell structure retards the H uptake during charging and hence reduces H-induced hardening. Nanoindentation experiments along with thermal desorption analysis were utilized to elucidate the mechanistic reasons behind this unique behavior.

The SLM 316L SS coupons (2.5 × 15.7 × 30 mm^3 each, in size) were fabricated in a commercial M2 powder-bed fusion machine (Concept Laser GmbH, Lichtenfels, Germany) equipped with a 400 W fiber laser in argon environment. SLM was conducted with laser beam size = 54 μm, hatch spacing = 105 μm, laser power = 150 W, and scan speed = 700 mm/s. The build layer thickness is 30 μm, and an island scan strategy [31] was applied. For comparison purpose, we also examined a commercial-grade, well-annealed 316L SS as reference material (referred to as "CM" hereafter), of which the chemical composition is listed along with that of SLM sample in Table S1 in Supplementary Material. The specimens were final-polished using VibroMet 2 polisher (Buehler, Lake Bluff, IL, USA) with 0.02 μm colloidal silica for 10 h. All the subsequent experiments performed on the SLM samples in the present study were conducted on the surface parallel to the build direction (i.e. the side surface). Electron backscattered diffraction (EBSD; e^-Flash^{FS}, Bruker Nano GmbH, Berlin, Germany) and transmission electron microscopy (TEM; Titan 80-300, FEI, Hillsboro, OR, USA) were utilized to characterize the crystal- and meso-structures.

The polished specimens were electrochemically H-charged [32] at room temperature (RT, ~25°C) and 50°C with a potentiostat/galvanostat equipment (HA-151A, Hokuto Denko, Tokyo, Japan) using a mixture of 0.1 mol/L NaOH and 0.5 wt.% NH_4SCN as the electrolytic solution. While various charging temperature and time were applied, the same current density of 5 mA/cm^2 was adopted for all the cases. Nanoindentation experiments with Berkovich tip were performed at both high load (peak load P_{max} = 100 mN, with indentation strain rate = 0.025 s^{-1}) using Nanoindenter-XP (formerly MTS; now KLA Corporation, Milpitas, CA, USA) and low load (P_{max} = 100 μN, with loading rate = 20 μN/s) using TI950 Triboindenter (formerly Hysitron; now Bruker Corp., Minneapolis, MN, USA). The specific location of each low-load indent was identified by recourse to forward-scattered electron (FSE) imaging, which utilizes an EBSD detector (e^-Flash^{HR}) equipped with a forward- and backscattered electron detection system (ARGUS^{TM}, Bruker Nano GmbH, Berlin, Germany). Thermal desorption spectroscopy (TDS) was employed for the quantitative analysis of the H content in the hydrogenated samples, using a gas chromatograph (JTF-20A, J-Science Lab Co. Ltd, Kyoto, Japan) with a constant heating rate of 100 °C/h.

The orientation and size distribution of grains in both samples were characterized by EBSD, and the obtained inverse pole figure (IPF) images are displayed in Fig. 1. The microstructure of CM 316L (Fig. 1a) consists of equiaxed grains with an average grain size, d, of ~33 μm. Since the CM alloy is well annealed, a low density of dislocations in it is expected. Fig. 1b exhibits the IPF map of the SLM 316L, and the d was determined to be ~45 μm. Note that the numerous low-angle grain boundaries (LAGBs) in the SLM sample [6] were not counted during the d estimation. Single face-centered cubic (fcc) phase of both CM and SLM samples was confirmed by X-ray diffraction (XRD) results (see Fig. S1 in Supplementary Material). Fig. 2a shows a high-angle annular dark-filed (HAADF) image of SLM sample obtained in the scanning TEM (STEM) mode. Fine cellular structure embedded within individual grains can be seen. The size of the cells is nonuniform, ranging from 0.2 to 1.0 μm in average spacing in the same sample [12]. A closer examination via bright-filed (BF) TEM (Fig. 2b) reveals that the cell walls contain a

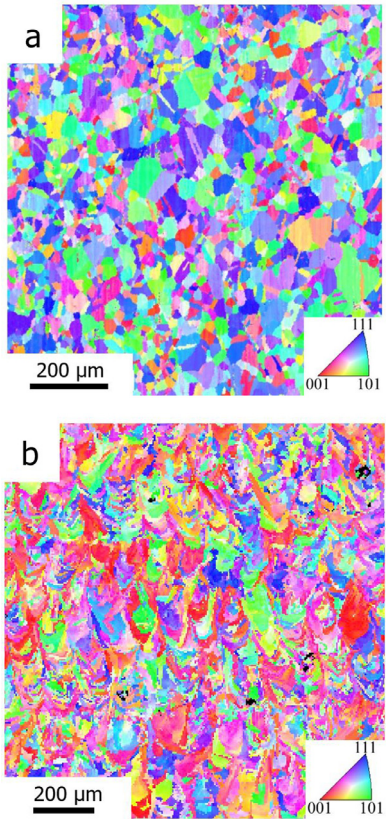

Fig. 1. Representative EBSD inverse pole figure (IPF) maps of (a) CM and (b) SLM 316L samples. Note the differences in the scale bars of the two images.

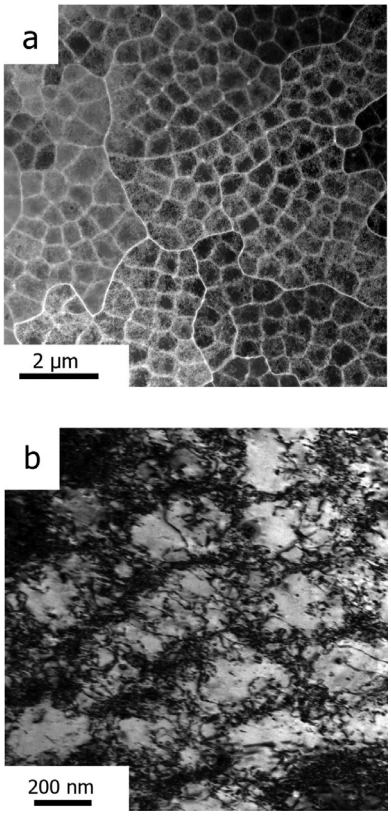

Fig. 2. Transmission electron micrographs showing the solidification cellular structure in the SLM 316L specimens. (a) HAADF TEM image of the solidification cells, and (b) bright field TEM image showing a high density of dislocations in the cell walls.

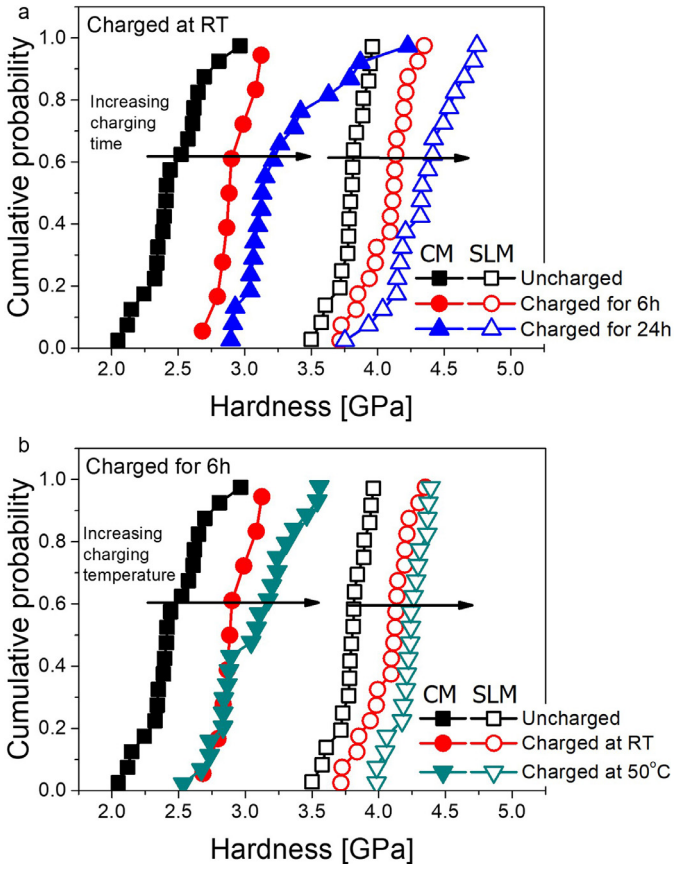

Fig. 3. Cumulative probability distribution of the hardness values obtained on SLM and CM 316L SS specimens before and after charging for (a) different time and (b) at different temperatures.

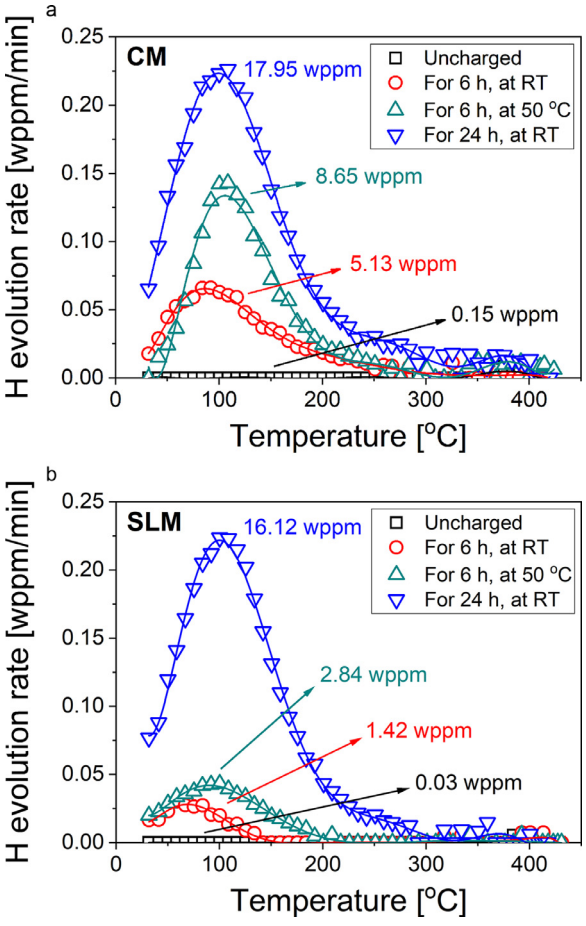

Fig. 4. Thermal desorption spectra obtained on the H-charged (a) CM and (b) SLM 316L samples. Lines are drawn through the data for the purpose of guiding the eye.

high density of dislocations. Such a solidification cell structure is widely reported in the SLM SSs [6,30,33]. Segregation of elements, mainly Cr and Mo, to the dislocation walls was observed with the aid of compositional mapping in Refs. [6,7].

From the nanoindentation tests conducted at P_{max} = 100 mN, variations in the hardness values for both uncharged and H-charged samples of CM and SLM 316L are presented in Fig. 3 in terms of cumulative probability distributions. In the uncharged condition, the hardness of SLM sample is much higher than that of the CM sample. The higher hardness of SLM 316L is primarily due to the fine cellular structure in it [6,7,34], either by being an obstacle to dislocation movement (then leading to Hall-Petch-like dependence of strength on cell size) [6] or simply by cell wall's high-density dislocations (following Taylor strengthening for forest dislocations) [34]. By comparing the hardness in uncharged and charged states, it is clear that both the time (Fig. 3a) and temperature (Fig. 3b) of charging enhance the hardness of both CM and SLM samples [35]. Table 1 summarizes the average hardness values of the uncharged (H_U) and charged (H_C) samples, the difference between them ($\Delta H = H_C - H_U$), and the normalized percentage of hardness increment ($\Delta H/H_U$). In all the charged conditions, the SLM alloy always shows both smaller ΔH and smaller $\Delta H/H_U$ than the CM 316L, suggesting SLM 316L alloy is less sensitive to H charging.

TDS measurements were employed to gain insights into the correlation between the H content and the observed differences in the hardening behavior of CM and SLM 316L samples. As displayed in Fig. 4, in both uncharged samples of CM and SLM, the amount of H, which may come from manufacturing process, is negligible (~0.15 and 0.03 wppm, respectively). With an increase in either time or temperature of H charging, the H content in each sample increases. Since hardness also changes in the same manner (Fig. 3), this observation suggests that the only possible reason for the observed hardening is H-induced mechanisms. Such hardening has been usually explained by general solid solution strengthening mechanisms such as dislocation dragging or pinning [36] and H-enhanced slip planarity [37].

Table 1
The average hardness values for uncharged (H_U), charged (H_C) samples, the hardness increment ($\Delta H = H_C - H_U$), and the normalized hardness increment ($\Delta H/H_U$) for CM and SLM 316L SS samples.

	Uncharged	Charged for 6 h, RT			Charged for 6 h, 50°C			Charged for 24 h, RT		
	H_U	H_C	ΔH	$\frac{\Delta H}{H_U}$	H_C	ΔH	$\frac{\Delta H}{H_U}$	H_C	ΔH	$\frac{\Delta H}{H_U}$
CM	2.45	2.91	0.46	18%	3.05	0.60	24%	3.28	0.82	34%
AM	3.79	4.07	0.28	7%	4.22	0.43	11%	4.32	0.54	14%

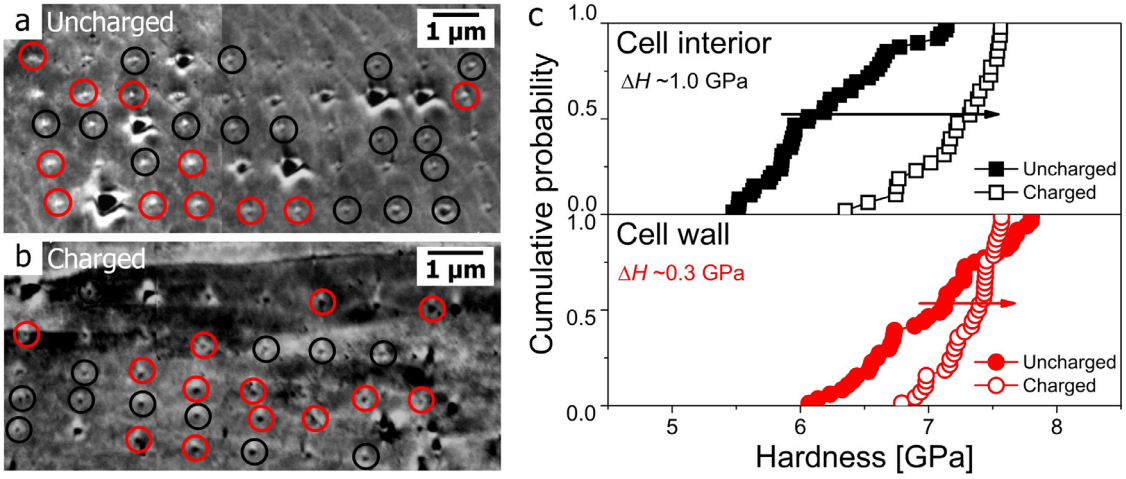

Fig. 5. Representative FSE images showing the low-load nanoindentation arrays on (a) uncharged and (b) charged AM 316L samples (the indents marked with black circles are those made on cell interiors, while those circled with red correspond to cell walls). (c) Cumulative distributions of hardness values obtained on cell interiors (top plot) and walls (bottom plot) in both uncharged and charged AM 316L samples.

For identical charging conditions, the H content in the CM alloy is about three times that in the SLM alloy after 6 h charging, whereas only marginal difference in H content exists after 24 h charging. Recent study on 304L austenitic SS showed that SLM and CM alloys possess similar H content after prolonged H charging (5 days) [19]. This suggests that SLM 316L may also possess a similar steady-state H solubility as that of the CM alloy whereas the H diffusivity is largely reduced in the former; i.e., while H content after 6 h charging is much lower in the SLM alloy due to the low H diffusivity in it, the gap in the H contents between SLM and CM samples is reduced after long time charging at or near saturation conditions. This is contrary to the prior studies on austenitic SSs which reported an increase in H absorption with increasing dislocation density [23,38]. Since the solidification cell structure is a key microstructural feature that is different in these two steels, it is reasonable to attribute the different behavior noted in the SLM alloy to this feature. Unlike typical dislocations in conventional metals and alloys, the dislocation-tangled cell walls are energetically stable [34], which is attributed to the pinning effect from the segregated elements and/or oxides in cell walls [6]. Such stability leads to an invariance of the characteristic size and shape of the cells even after plastic deformation [7] or thermal annealing [30,39]. Because of the relatively stable state of the cell walls, it is possible that their potential energy landscape for H is shallower than that of typical microstructural defects and possibly comparable to that of the interstitial lattice sites. Such shallow potential well makes the walls unfavorable residing sites for H, which is a distinct feature from the typical dislocations in CM alloys

In Fig. 5, another noticeable feature lies in the temperature spans over which the desorption peaks occur are different in the CM and SLM alloys. While the temperature at which the H evolution rate becomes zero, T_0, is ~300 (for 6 h) or ~400°C (for 24 h) in the CM alloy, T_0 becomes ~150-200 (for 6 h) or ~300°C (for 24 h) in the SLM alloy. In fcc metals, H diffusion, which is slower than the detrapping process, is the rate-controlling mechanism during the thermal desorption process [23,40]. Therefore, T_0 can be directly correlated to the maximum depth to which H atoms penetrate during charging, or H diffusivity. On this basis, the observed higher T_0 (and thus a deeper distance reached by H atoms through diffusion) in CM samples than in SLM samples further confirms the relatively lower H diffusivity in the latter. This, in turn, implies that the cell structure in the SLM alloy is effective in impeding the diffusion of H. This is also contrary to the observations in conventional austenitic SSs where the dislocation density does not alter the H diffusivity in a significant manner [38,41]. A comparison of the H diffusivity (D_H) data of SLM 316L, obtained by gas-phase permeation tests [42], with that of the CM 316L available in literature [23,43–45], is made in Table S2 in Supplementary Material. While D_H of SLM and CM alloys, both at RT and at 50°C, are similar in magnitude, the former is slightly lower than all those reported for CM 316L. Since the cell walls densely distributed everywhere in the SLM sample are not preferable for H atoms' residence, the H diffusion process by hopping of H atoms between interstitial lattice sites [46] may be effectively blocked by those walls, leading to less number of diffusion paths available for H atoms and hence the reduced the apparent H diffusivity.

To further elucidate the cellular structure's role in the observed hardening in H-charged SLM samples, low-load nanoindentation tests ($P_{max} = 100\ \mu$N, with the maximum displacement always less than 20 nm) were performed on both uncharged and 24 h charged SLM samples. To ascertain whether a specific indent is located on the cell well or interior, FSE imaging was utilized. Representative examples of the obtained FSE images are presented in Fig. 5a and 5b where the cellular structure is visible. At least 24 points corresponding to either cell interior or wall were obtained, of which the hardness results are displayed in Fig. 5c. The indents located right on cell wall or interior were categorized and the average hardness results were obtained. In the uncharged condition, the average hardness of the cell walls is ~12% higher than the cell interior, as expected. Upon charging, while cell interiors harden significantly (ΔH ~1.0 GPa and $\Delta H/H_U$ ~16%), the cell walls only show a marginal hardness increase (ΔH ~0.3 GPa with $\Delta H/H_U$ ~4%). This marginal changes in hardness of the cell walls upon H charging can be attributed to either lower H content in the walls, or the difficulty in hardening the already-hardened cell walls, or both. Either way, it leads us to conclude that the well-developed cell structure in AM 316L does not cause a substantial H-induced strengthening.

For relatively "stable" austenitic SSs like 316L that are not susceptible for martensitic transformation (no evidence for phase transformation was detected in our H-charged specimens), the widely-accepted micromechanisms of H embrittlement is H-enhanced localized plasticity (HELP) [25,47]. For the HELP mechanism, both H solubility and diffusivity are essential in determining the existence and/or magnitude of H embrittlement in austenitic SSs as both these factors affect the local H content in critical regions (such as crack tip) [48,49]. In this context, the findings of the present study, namely effective reduction in H diffusivity and H-induced hardening caused by the cellular structure, indicate that

SLM 316L alloy is likely to be less susceptible to H embrittlement. A CM 316L alloy with a comparable high dislocation density (obtained, for instance, by cold rolling) is likely to show inferior HE resistance due to the enhanced solubility while the diffusivity of H does not get affected [38,41]. Therefore, the SLM 316L alloy may be a promising candidate in industrial applications where H environment is prevalent.

In summary, although the intrinsic hardness of SLM 316L steel is much higher than that of an annealed CM steel, the hardness enhancement due to H charging in the former is lower than in the latter. Through TDS analyses, it was revealed that the solidification cell structure in the SLM alloy reduces the apparent H diffusivity but has insignificant effect on the H solubility, indicating that the high-density of dislocations present in the cell walls are essentially different in nature from the randomly-distributed dislocations in conventional alloys. By recourse to low-load nanoindentation experiments with FSE imaging, the cell walls are proven to be more resistant to H absorption and hence hardening, as compared to the cell interiors. The observations in the present study suggest a promising characteristic of the SLM alloys in resisting H-induced mechanical degradation.

Declaration of Competing Interest

The authors declare that they have no known competing financial interests or personal relationships that could have appeared to influence the work reported in this paper.

Acknowledgements

The work at Hanyang University was supported by the National Research Foundation of Korea (NRF) grants funded by the Korea government (MSIT) (No. 2020R1A2B5B01001446 and No. 2020R1A5A6017701). The work at the Nanyang Technological University was supported by the funding from A*STAR via the Structural Metals and Alloys Programme (No. A18B1b0061). The work at the Lawrence Livermore National Laboratory (LLNL) was performed under the auspices of DOE contract No. DE-AC52-07NA27344. T. Voisin and Y.M. Wang acknowledge the support of the Laboratory Directed Research and Development (LDRD) program (20-SI-03) at LLNL.

Supplementary materials

Supplementary material associated with this article can be found, in the online version, at doi:10.1016/j.scriptamat.2020.113718.

References

[1] D. Herzog, V. Seyda, E. Wycisk, C. Emmelmann, Acta Mater 117 (2016) 371–392.
[2] P. Kumar, R. Jayaraj, J. Suryawanshi, U.R. Satwik, J. McKinnell, U. Ramamurty, Acta Mater 199 (2020) 225–239.
[3] P. Kumar, O. Prakash, U. Ramamurty, Acta Mater 154 (2018) 246–260.
[4] J. Suryawanshi, K.G. Prashanth, S. Scudino, J. Eckert, O. Prakash, U. Ramamurty, Acta Mater 115 (2016) 285–294.
[5] O. Nenadl, V. Ocelík, J.T.M. De Hosson, J. Laser Appl. 29 (2017) 042007.
[6] Y.M. Wang, T. Voisin, J.T. McKeown, J. Ye, N.P. Calta, Z. Li, Z. Zeng, Y. Zhang, W. Chen, T.T. Roehling, R.T. Ott, M.K. Santala, P.J. Depond, M.J. Matthews, A.V. Hamza, T. Zhu, Nat. Mater. 17 (2018) 63–70.
[7] L. Liu, Q. Ding, Y. Zhong, J. Zou, J. Wu, Y.L. Chiu, J. Li, Z. Zhang, Q. Yu, Z. Shen, Mater. Today 21 (2018) 354–361.
[8] Q. Jia, D. Gu, J. Alloys Compd. 585 (2014) 713–721.
[9] V. Ocelík, N. Janssen, S.N. Smith, J.T.M. De Hosson, JOM 68 (2016) 1810–1818.
[10] Z.G. Zhu, X.H. An, W.J. Lu, Z.M. Li, F.L. Ng, X.Z. Liao, U. Ramamurty, S.M.L. Nai, J. Wei, Mater. Res. Lett. 7 (2019) 453–459.
[11] J. Suryawanshi, K.G. Prashanth, U. Ramamurty, Mater. Sci. Eng. A 696 (2017) 113–121.
[12] Z. Li, T. Voisin, J.T. McKeown, J. Ye, T. Braun, C. Kamath, W.E. King, Y.M. Wang, Int. J. Plast. 120 (2019) 395–410.
[13] T. DebRoy, H.L. Wei, J.S. Zuback, T. Mukherjee, J.W. Elmer, J.O. Milewski, A.M. Beese, A. Wilson-Heid, A. De, W. Zhang, Prog. Mater. Sci. 92 (2018) 112–224.
[14] K. Chen, R. Huang, Y. Li, S. Lin, W. Zhu, N. Tamura, J. Li, Z. Shan, E. Ma, Adv. Mater. 32 (2020) 1907164.
[15] S.W. Baek, E.J. Song, J.H. Kim, M. Jung, U.B. Baek, S.H. Nahm, Scr. Mater. 130 (2017) 87–90.
[16] R. Silverstein, D. Eliezer, Mater. Charact. 144 (2018) 297–304.
[17] Y.J. Kwon, R. Casati, M. Coduri, M. Vedani, C.S. Lee, Materials (Basel) 12 (2019) 1–12.
[18] X. Li, Q. Li, T. Wang, J. Zhang, Corros. Sci. 160 (2019) 108171.
[19] D.-H. Lee, B. Sun, S. Lee, D. Ponge, E.A. Jägle, D. Raabe, Mater. Sci. Eng. A (2020) In press, doi:10.1016/j.msea.2020.140499.
[20] J.P. Hirth, Metall. Trans. A 11 (1980) 861–890.
[21] Y. Zhao, D.-H. Lee, M.-Y. Seok, J.-A Lee, M.P. Phaniraj, J.-Y. Suh, H.-Y. Ha, J.-Y. Kim, U. Ramamurty, J.-I. Jang, Scr. Mater. 135 (2017) 54–58.
[22] M. Dadfarnia, A. Nagao, S. Wang, M.L. Martin, B.P. Somerday, P. Sofronis, Int. J. Fract. 196 (2015) 223–243.
[23] C. San Marchi, B.P. Somerday, S.L. Robinson, Int. J. Hydrogen Energy 32 (2007) 100–116.
[24] Y. Zhao, J.-M. Park, D.-H. Lee, E.J. Song, J.-Y. Suh, U. Ramamurty, J.-I. Jang, Scr. Mater. 168 (2019) 76–80.
[25] H.K. Birnbaum, P. Sofronis, Mater. Sci. Eng. A 176 (1994) 191–202.
[26] U. Ramamurty, J.-I. Jang, CrystEngComm 16 (2014) 12–23.
[27] G. Yang, Y. Zhao, D.-H. Lee, J.-M. Park, M.-Y. Seok, J.-Y. Suh, U. Ramamurty, J.-I. Jang, Scr. Mater. 161 (2019) 23–27.
[28] W.A. Soer, K.E. Aifantis, J.T.M. De Hosson, Acta Mater 53 (2005) 4665–4676.
[29] W.A. Soer, J.T.M. De Hosson, A.M. Minor, J.W. Morris, E.A. Stach, Acta Mater 52 (2004) 5783–5790.
[30] T. Voisin, J. Forien, A. Perron, S. Aubry, N. Bertin, A. Samanta, A. Baker, Y.M. Wang, Acta Mater 203 (2021) 116476.
[31] L.N. Carter, C. Martin, P.J. Withers, M.M. Attallah, J. Alloys Compd. 615 (2014) 338–347.
[32] Y. Zhao, M.-Y. Seok, I.-C. Choi, Y.-H. Lee, S.-J. Park, U. Ramamurty, J.-Y. Suh, U. Ramamurty, J.-I. Jang, Scr. Mater. 107 (2015) 46–49.
[33] K.G. Prashanth, J. Eckert, J. Alloys Compd. 707 (2017) 27–34.
[34] Z. Li, B. He, Q. Guo, Scr. Mater. 177 (2020) 17–21.
[35] Y. Yao, X. Pang, K. Gao, Int. J. Hydrogen Energy 36 (2011) 5729–5738.
[36] A. Barnoush, M. Asgari, R. Johnsen, Scr. Mater. 66 (2012) 414–417.
[37] K.A. Nibur, D.F. Bahr, B.P. Somerday, Acta Mater 54 (2006) 2677–2684.
[38] Y. Mine, C. Narazaki, K. Murakami, S. Matsuoka, Y. Murakami, Int. J. Hydrogen Energy 34 (2009) 1097–1107.
[39] M. Shamsujjoha, S.R. Agnew, J.M. Fitz-Gerald, W.R. Moore, T.A. Newman, Metall. Mater. Trans. A Phys. Metall. Mater. Sci. 49 (2018) 3011–3027.
[40] S.M. Lee, J.Y. Lee, Metall. Trans. A, Phys. Metall. Mater. Sci. 17 A (1986) 181–187.
[41] T.-P. Perng, C.J. Altstetter, Acta Metall 34 (1986) 1771–1781.
[42] J. Lin, F. Chen, F. Liu, D. Xu, J. Gao, X. Tang, Mater. Chem. Phys. 250 (2020) 123038.
[43] A.M. Brass, J. Chene, Mater. Sci. Eng. A 242 (1998) 210–221.
[44] S.K. Lee, S.H. Yun, H.G. Joo, S.J. Noh, Curr. Appl. Phys. 14 (2014) 1385–1388.
[45] N. Kishimoto, T. Tanabe, T. Suzuki, H. Yoshida, J. Nucl. Mater. 127 (1985) 1–9.
[46] A. Turnbull, in: Gaseous Hydrog. Embrittlement Mater. Energy Technol. Mech. Model. Futur. Dev., Woodhead Publishing, 2012, pp. 89–128.
[47] C.San Marchi, Int. J. Hydrogen Energy 33 (2008) 889–904.
[48] D.G. Ulmer, C.J. Altstetter, Acta Metall. Mater. 39 (1991) 1237–1248.
[49] D.P. Abraham, C.J. Altstetter, Metall. Mater. Trans. A 26 (1995) 2849–2858.